Noname manuscript No.
(will be inserted by the editor)

Fast in silico assessment of physical stress for peripheral nerves

[*]**Elisabetta Giannessi** · **Maria Rita Stornelli** ·

[†*]**Pier Nicola Sergi**

[*] **equally contributors** [†] **corresponding author**

Received: date / Accepted: date

Abstract The level of physical stress rules the adaptative response of peripheral nerves, which is crucial to assess their physiological and pathological states. To this aim, in this work, different computational approaches were presented to model the stress response of *in vitro* peripheral nerves undergoing longitudinal stretch. More specifically, the effects of geometrical simplifications were studied with respect to the amount of computational time needed to obtain relevant information. Similarly, the variation of compressibility of the peripheral nervous tissue was investigated with respect to the variation of longitudinal stress and transversal stretch variations, and with reference to the computational time needed for simulations. Finally, the effect of small dimensional changes was investigated to better understand whether the variation of time was only due to the amount of nodes or elements. In conclusion, since fast in silico models, able to assess the nerve stress could be a strategic advantage in case of time constraints or on-line evaluation (e.g., surgical interventions)

Elisabetta Giannessi ([*] equally contributor)
Department of Veterinary Science, University of Pisa, Pisa, Italy.

Maria Rita Stornelli
Department of Veterinary Science, University of Pisa, Pisa, Italy.

Pier Nicola Sergi ([*] equally contributor and [†] corresponding author)
The Biorobotics Institute, Scuola Superiore Sant'Anna, Viale Rinaldo Piaggio 34, Pontedera, 56025, Italy.
Tel: +39 050 88 3059
Fax: +39 050 88 3101
E-mail: p.sergi@sssup.it//pn.sergi@gmail.com

a synergistic use of these approaches was proposed as a possible strategy to decrease the computational time needed for simulations from minutes to seconds.

Keywords Peripheral nerves, Physical stress, Fast in silico models

1 Introduction

Peripheral nerves are composite structures [38, 39] able to transport electrical signals from the brain to the periphery of the body. They are quite easily stretchable within a physiological range [9, 10], to maintain the structural continuity of internal fibers. Indeed, within the nerve trunk, axons show a redundant undulated shape [45], which results in the optical phenomenon of the bands of Fontana [7, 17, 21, 22, 44]. In addition, an irregular network of capillaries [45], supplies each nerve from adjacent blood vessels and provides both collateral and segmental circulation [35, 36]. However, some situations (e.g., injuries) could lead to supraphyisiological stretches, which are able to smoothen undulated axons and to damage vasa nervorum [3]. In other words, stretch injuries, which are among the "most common" human nerve injuries [45], could involve a combination of ischemic and mechanical damages, due to the simultaneous destruction of the epineural plexus and to the mechanical distortion of axons [45].

In addition, intra-epineural sclerosis and extraneural constriction were described as adverse effects associated to the nerve stimulation [37], while complications due to peripheral nerve overstretch were described in surgical procedures for bone reconstruction [13] (e.g., Iliazarov procedure [16]). Furthermore, the physical stress of a nerve was related to their adaptative response to the external environment [25, 41]. Nevertheless, stretch injuries are among the "least studied" form of injuries [45], thus the knowledge of the stress field, arising within the stretched nerve, is crucial to account for their physiological and pathological states.

Experiments and in silico models were both used to investigate pathological conditions of peripheral nerves or their interaction with external devices. More specifically, piglet nerves were studied to explore the unilateral vocal fold paralysis [42], while interactions between peripheral nervous tissue (PNT) and tungsten microneedles [30, 31, 43] were studied

to improve the insertion of intraneural interfaces [8, 28]. Finite Elements (FE) models were used to reproduce the subject specific geometry of specimens [2, 4, 11, 14, 20, 26, 34, 40]. Nevertheless, a different approach could be desirable in case of time constraints, as real time interventions or the assessment of a surgical procedure for many patients, where, a fast in silico approach, able to quickly assess the needed information, could be strategic. To this aim, the effects of geometrical simplification, variation of compressibility and dimensional approximation were explored in this work.

2 Materials and Methods

2.1 Experiments

A sciatic nerve (65mm long) was dissected from a posterior limb of a Large White pig ($\sim$ 10 months old), which was slaughtered in conformity with the National Italian Regulation and frozen until experiments. According to literature [15], the nerve specimen was gradually defrosted and re-hydrated for about one hour at room temperature in a bath of aqueous saline solution (0.9% sodium chloride isotonic to the blood) before experiments. The physiological characteristics (e.g., stiffness) of the specimen (which had a length between clamps of 55mm), were preserved by spraying saline solution on its surface. Stretch experiments were performed at room temperature ($\sim 25 \pm 1^{\circ}C$), by using an Instron R4464 testing machine (Instron Corporation, Canton, MA) with a standard load cell (Instron load cell, Instron Corporation, cell type $2525-808$, max force 10 N, accuracy 0.25% Full Scale Output). The nerve was longitudinally stretched (velocity $v = 10mm/min$; maximum stretch 8%) after preconditioning to minimize viscoelastic effects [12] and the axial force was digitally recorded (see Figure 1).

Figure 1 about here

2.2 Theoretical background

The peripheral nervous tissue (PNT) was modelled as homogeneous and incompressible and, according to the literature [1, 18, 19, 42], its behaviour was assumed to derive from a

strain energy function Ψ^*, which was defined, in terms of principal invariants, as:

$$\Psi^*(I_1,I_2,I_3) = \Psi(I_1,I_2) - \frac{k}{2}(I_3-1) \tag{1}$$

where k was an indeterminate Lagrange multiplier accounting for boundary conditions and the principal strain invariants I_1,I_2,I_3 were respectively defined as: $I_1(\mathbf{b}) = tr\mathbf{b}, I_2 = \frac{1}{2}[(tr(\mathbf{b})^2) - tr(\mathbf{b}^2)], I_3(\mathbf{b}) = det(\mathbf{b})$. In addition, $\mathbf{b} = \mathbf{F}\mathbf{F}^\mathbf{T}$ was the left Cauchy-Green tensor, while $\mathbf{F}$ was the deformation gradient. The PNT was assumed to be incompressible, thus $I_3 = 1$, and the transversal stretch was defined as $1/\sqrt{\lambda}$, where λ was the longitudinal stretch. Therefore, the Cauchy stress was:

$$\sigma = -k\mathbf{I} + 2\frac{\partial\Psi(I_1,I_2)}{\partial I_1}\mathbf{b} - 2\frac{\partial\Psi(I_1,I_2)}{\partial I_2}\mathbf{b}^{-1} \tag{2}$$

In particular, a suitable strain energy function, which was a generalization of [42], was written in the form:

$$\Psi(I_1,I_2) = \sum_{i=0}^{1}\sum_{j=0}^{1} c_{ij}(I_1-3)^i(I_2-3)^j \tag{3}$$

where $c_{ij} \in \Re$ were scalar coefficients. Finally, for computational purposes, the PNT was also modelled as a near incompressible material, thus the strain energy function was rewritten as:

$$\Psi^*(I_1,I_2,J) = \sum_{i=0}^{1}\sum_{j=0}^{1} c_{ij}(I_1-3)^i(I_2-3)^j + \frac{1}{d}(J-1)^2 \tag{4}$$

where $d = 2/K$ was a variable accounting for the material compressibility, K was the material bulk modulus and $J = det(\mathbf{F})$.

2.3 In silico approaches

The in silico models of the nerve were implemented though a standard FE software (Ansys © Academic, Ansys, Inc. Canonsburg, Pennsylvania, USA). First, a suitable approximation

of the three-dimensional nerve geometry was obtained by reproducing each profile with ImageJ (National Insitutes of Health, USA) and by computing the resulting mean straight lines. The real specimen geometry was, then, approximated with an elliptical cylinder, whose major and minor axes were respectively 4.52 mm and 1.38 mm long. This structure was meshed with solid elements (SOLID185), which were able to account for fully incompressible hyperelastic materials through enhanced strain and mixed displacement-pressure formulation. This procedure resulted in 2016 nodes and 1375 elements. Since the eccentricity of the specimen cross section was 0.95, the previous cylindroid was approximated with a tape like structure, with a rectangular section of 2.76 mm and 9.05 mm. The specimen was, therefore, modelled as a parallelepiped, which was meshed with 2464 nodes and 1650 elements.

Furthermore, low dimensional models were implemented, exploiting the plane stress approximation of the whole structure. In particular, the parallelepiped was further reduced to its middle plane, which coincided with the symmetry plane along the structure depth (z axis). Then, eight-nodes plane elements (PLANE 183), allowing each node to have two translational degrees of freedom, were used to mesh this plane. The meshing procedure resulted in 1781 nodes and 550 elements. In all these cases, the lower area or line, belonging to the model, was fully constrained to account for experimental constrains, while increasing displacements were imposed to the upper extremity to closely mimic the experimental stretches. The global times for the solution of the three-dimensional models as well as for plane stress approximations (with and without thickness) were compared and eventual differences in stress fields were investigated.

Moreover, the PNT was modelled as a nearly incompressible material, since the compressibility was set to be $d = 1E-010$, $d = 1E-009$, $d = 1E-008$, $d = 1E-007$, $d = 1E-006$, $d = 1E-005$. The performances of these models were compared to the fully incompressible case (i.e., $d = 0$) with respect to the stress field, the lateral stretch, and the computational time needed to solve the model.

Furthermore, the effects of the dimensional approximation were studied. More specifically, the lateral dimension of the bidimensional plane stress model were slightly changed with respect to the reference (bidimensional) model (i.e., width=9.05 mm). This dimension

were slightly increased (up to 9.1 mm) or decreased (up to 9.0 mm). The effects on the computational time were studied.

3 Results

In Figures 2a, 2b the spatial distribution of displacement and stress at the maximum stretch (i.e., $\lambda = 1.08$) is shown for the threedimensional model of nerve with elliptical section. This model was able to reproduce the experimental relationship between stress and stretch in axial direction ($R^2 \simeq 0.9$) for $c_{01} = 0.9702$ KPa, $c_{10} = 0.4998$ KPa, $c_{11} = 49.294$ KPa, with a maximum percentage error within the 4.5%, as shown in Figures 2c, 2d. Similarly, this model was able to reproduce the transversal stretch of the specimen along the whole stretch range with a maximum error of $8E-004$, as shown in Figures 2e, 2f.

Figure 2 about here

In Figure 3a, the displacement field for an approximate models is shown. First, because of the eccentricity of the cylindrical specimen, a rectangular section was used to simplify its cross sectional area (on the left). Then, a planar reduction of the solid model was used to reproduce the displacement field (Figure 3a, right). Similarly, the stress field was computed for the parallelepiped (Figure 3b, left) and for the bidimensional approximation (Figure 3b, right).

Figure 3 about here

The behaviour of these approximate geometries was compared to the performances of the cylindroid, which was used as a reference, since it was able to reproduce the experimental results. The relationship between stretch and axial stress was investigated for all the approximations (i.e., parallelepiped, plane with thickness and plane without thickness) and, in all cases, it was superimposed to the reference curve in the whole range of stretches, as shown in Figure 4a. To quantify the reliability of the different models to reproduce the cylindroid performances, the percentage error was computed and resulted within the 0.003% (Figure 4b). Similarly, the transversal stretch was investigated for all the approximate models (Figure 4c) and resulted in differences within 0.0004, as shown in Figure 4d.

Figure 4 about here

Moreover, the influence of the compressibility on axial stress was investigated. In Supplementary Figure 1a, different values of compressibility (ranging from $d = 1E-005$ to $d = 1E-010$) were compared to the fully incompressible case (d=0) for the elliptic cylindroid. The errors resulted within $4.5E-005$ KPa, as shown in Supplementary Figure 1b. Similarly, the effects of the variation of compressibility were investigated for the parallelepiped and for both the plane stress approximation with and without thickness. The comparison to the fully incompressible case is shown in Supplementary Figures 1c, 1e, 1g, while the differences with the fully incompressible case were reported in Supplementary Figures 1d, 1f, 1h, respectively for the parallelepiped, the bidimensional rectangle with thickness and the bidimensional rectangle without thickness. Also in these cases, the maximum errors were within $6E-005$ KPa.

The effects of compressibility on the transversal stretch were also studied. More specifically, in Supplementary Figures 2a, 2b the difference between the fully incompressible case and the near incompressible ones was investigate for $d = 0$, $d = 1E-010$, $d = 1E-009$, $d = 1E-008$, $d = 1E-007$, $d = 1E-006$, $d = 1E-005$. All the curves were superimposed (Supplementary Figure 2a) and the maximum difference resulted within $1.4E-006$. For the other approximations, the results were similar, as shown in Supplementary Figures 2c, 2d, 2e, 2f, 2g, 2h, respectively for the parallelepiped, the plane with thickness and the plane without thickness.

In addition, the variation of the computational time needed to solve the in silico model was studied for different values of the compressibility parameter (d). All these times were normalized with respect to the computational time needed to solve the respective fully incompressible cases. More specifically, in Figure 5a, the maximum percentage decrease (i.e., 2.27%) for the threedimensional cylindroid is shown for $d = 1E-005$, similarly for the threedimensional parallelepiped (Figure 5b) the maximum decrease of computational cost (i.e.,0.80%) was achieved for $d = 1E-005$. Instead, for bidimensional approximations (plane stress with or without thickness) the maximum values (i.e., respectively 81.96% and 81.41%) were both achieved for $d = 1E-007$, as shown respectively in Figures 5c

and 5d. Finally, the percentage decrease of computational time of each different model was compared to the time needed to solve the fully incompressible cylindroid, as shown in Figure 5e. The maxima of time decrease were achieved for the near incompressible bidimensional model without thickness (i.e., 97.18%), as well as for the near incompressible bidimensional model with thickness (i.e., 97.25%). In both these cases the compressibility was $d = 1E-007$.

Figure 5 about here

To further explore the sensitiveness of the bidimensional models with respect to the degree of numeric approximation, the amount of nodes and elements was computed for a width varying between 9.000 mm and 9.100 mm, while the length was kept constant (i.e., 55 mm). More specifically, these values were normalized with respect to the amount of nodes and elements of the main bidimensional approximations (i.e., width = 9.05 mm). Both values (nodes and elements) are lower (respectively 0.906 and 0.900 for nodes and elements) for the lower dimension, while were kept constants (i.e., 1) for all the other approximations, as shown in Figure 6a. The computational time needed to solve the whole cycle was, therefore, computed for different values of width and compressibility and normalized with respect to the time needed to solve the main approximation (i.e., width=0.95 mm). In particular, for a fully incompressible material $d = 0$, and for the following values of width 9.000 mm, 9.040 mm, 9.045 mm, 9.04999 mm, 9.050 mm, 9.055 mm, 9.100 mm, the normalized times were, respectively 1.582,1.241,0.992,1.700,1.000,1.181,0.923, as shown in Figure 6b. Similarly, for the same values of width, but for a compressibility of $d = 1E-007$, these values were 0.987,0.995,0.985,0.995,1.000,0.984,0.992, as shown in Figure 6c.

Figure 6 about here

4 Discussion

The coupling between computer simulations and biological and medical investigations is becoming an emergent scientific paradigm. Indeed, thanks to the increasing of computational power, the behaviour of cells and tissues can be reproduced in silico with a great precision. In this work, the response of a sciatic nerve to longitudinal stretch was reproduced through

in silico models. First, to test a feature-based approach the specimen was approximated with a three-dimensional solid (cylindroid) of hyperelastic and fully incompressible material [24, 31, 42], whose coefficients (Mooney-Rivlin formulation with three constants) were obtained through a standard fitting procedure. This model was able to reproduce the experimental axial stress ($R^2 \simeq 0.9$, and maximum difference within 4.5%) and the transversal stretch (maximum difference within $8E-004$), but computational times were suitable for an off-line analysis, to be performed without time constraints. To investigate other solutions the geometry of the real specimen was simplified, thus the cylindroid was approximated with a parallelepiped, since the eccentricity of the specimen was high (i.e., 0.95). In this case, the stress and stretch fields, previously obtained with the reference cylindroid, were closely reproduced, since the axial stress had a low percentage error (i.e., -0.005%), while the difference for the transversal stretch was within 0.0001. However, in this way, the amount of elements and nodes enlarged together with the computational time, which increased of about 20%. Therefore, since the width of the parallelepiped was greater than its depth (i.e., more than three times), two plane stress approximations (with and without thickness), accounting for the behaviour of the mean section, were used to reproduce the response of the whole volume. Also in these cases, the errors with respect to the reference cylindroid were small for axial stress (within $\pm 0.002\%$) and for the transversal stretch (within -0.0004). In addition, the number of nodes and elements was smaller with respect to the previous three-dimensional models, so the computational time considerably decreased (i.e., about 80%).

4.1 Variation of compressibility

In parallel to this way, the effects of the variation of the compressibility were explored. In particular, the PNT was modelled as a near incompressible material, with quite low coefficient of compressibility d (i.e., d ranging from $1E-005$ to $1E-010$). For all models the axial stress was not influenced by compressibility changes (errors $1E-005$ KPa), as well as the transversal stretches (errors around 0.0008%). However, the computational time varied. Indeed, for three-dimensional models the decrease of time was small and oscillating around the 2% for the cylindroid, while it was in the range -2% , $+1\%$ for the parallelepiped. In

other words, in this case, the time needed to solve the near incompressible model was, for a very low compressibility, greater than the time needed to solve the fully incompressible case. This effect could be due to numerical causes. On the contrary, the variation of d was highly effective for bidimensional models, which showed in both cases (plane stress with and without thickness) a big time reduction (i.e., around 80%) with respect to the fully incompressible bidimensional approximations. In other words, the variation of compressibility was able to keep both axial and transversal response of the nerve (stress, stretch), while it was able to lower the computational time particularly for bidimensional models.

The plots of time decrease had flat (or near flat) portions (see Figure 5). As a consequence, even if a single maximum was localized, this value may have, at least, one comparable value. In particular, for the reference case (three-dimensional cylindroid) the maximum percentage decrease of computational time (i.e., 2.27% for $d = 1E-005$) was similar to the value achieved for $d = 1E-009$ (i.e., 2.20%), while the maximum time decrease for the three-dimensional parallelepiped (i.e., 0.80%) was not too different from the values achieved for $d = 1E-006$ and $d = 1E-007$, which were respectively 0.635 and 0.627. Similarly, for the plane stress approximations (with and without thickness) the maximum reductions of time were 81.41% and 81.96% for $d = 1E-007$, which were similar to the time reductions of 80.59% and 81.86%, which were obtained for $d = 1E-008$ respectively for plane stress with and without thickness. In other words, for a near incompressible material, whose the compressibility was in the range $1E-007, 1E-008$ the computational time was reduced in a similar way.

4.2 Is the reduction of computational time only due to the lower amount of nodes or elements ?

The parallelepiped was always more time expensive than the cylindroid as shown in Figure 5e. This was in agreement with the higher amount of its nodes and elements (i.e., 2464 nodes and 1650 elements) with respect to the reference cylindroid (i.e., 2016 nodes and 1375 elements). However, the amount of nodes of parallelepiped was the 22.22% higher, and the amount of elements was about 20% higher, while the extra time needed to solve the

model varied from 21.78% and 25.06%. As a consequence, there was an extra percentage ranging from $1-5\%$ due to other causes.

As previously shown, an effective strategy to decrease the computational time was to lower the dimensionality of the problem by using bidimensional models. Indeed, also in this case, both the number of nodes and elements were consistently lower, that is 1781 nodes and 550 elements. These values corresponded to a decrease of 11% in the amount of nodes and to a decrease of 59.7% in the amount of elements with respect to the reference geometry of the in silico specimen (cylindroid). Nevertheless, these values seem to be not enough to explain a decrease of computational time varying in the range $84.80\% - 97.25\%$, as shown in Figure 5e.

Again, some other causes seemed to be involved in the reduction of the needed computational time (i.e., a percentage ranging between $25\% - 85\%$). Very likely, in both cases the extra percentage of time decrease was due to the variation of the compressibility of the material, since the dimensions were kept. To further explore this problem for bidimensional models, and also to assess the sensitiveness to the variation of dimensions, the computational time was computed for different amounts of nodes and elements. As shown in Figure 6, the number of nodes and elements increased with dimensions (as expected), while the computational time had an oscillating behaviour. In particular, these variations were sensible to the degree of compressibility of the material. Indeed, for a fully incompressible material ($d = 0$) the normalized time needed was 0.986 for a width of (9.000 mm), while for the upper limit (9.100 mm) it was 0.992. Similarly, a difference between the reference case (time = 1) was found both for smaller (width=9.045 mm) and greater (width=0.955 mm) geometries, for which the normalized time were respectively 0.985 and 0.984. As expected, the variation for very similar dimensions (i.e., between width=9.4999 mm and width=9.050 mm) were small (i.e.,0.005) and the time needed was lower for the lower dimension.

Moreover, for a nearly incompressible material (i.e., $d = 1E-007$), the behaviour of the normalized time was again oscillating. Nevertheless, the magnitude of numeric oscillations with respect to the reference case was greater and the behaviour was quite different from the previous one. More specifically, for the lower dimension in the range (i.e, width=9.000 mm),

the normalized computational time was 1.581, while for the upper limit (i.e., width=9.100 mm), the needed time was 0.923. For small differences the oscillations were also evident. Indeed, although the normalized time was 0.992 and 1.181, respectively for width measuring 9.045 mm and 9.055 mm, this value was 1.700 for a width of 9.04999 mm. In other words, for a very small dimensional gaps there was a big difference in the normalized time. As shown in Figure 6c, also in this case the trend of the normalized time was not easily related to the variation of the number of nodes or elements.

5 Conclusions

The knowledge of the ”physical stress” of peripheral nerves is physiologically relevant since it drives their adaptation to the external environment [25, 41]. As a consequence, a procedure able to achieve a fast assessment of the stress field may be a strategic advantage in different branches of medicine and physical therapy [41].

A strategy involving geometrical simplifications, low dimensional in silico models, a near incompressible material, and a suitable numeric approximation was used to reduce the whole computational time of 97.25% with respect to the three-dimensional standard reference case. More specifically, the time needed to find the stress field within an elongating nerve (several steps from $\lambda = 1$ to $\lambda = 1.08$) was reduced from minutes to very few seconds keeping the some amount of information. This reductionist approach was suitable to quickly assess the gross physical stress [25] in a nerve and to predict its overall adaptative response (e.g., within a physiological or a pathological range of stretch) [41]. In addition, it could be also useful, in synergy with more complex models, to achieve precise initial guess to calibrate heavy computational models (as patient specific models) or the interaction between peripheral nerves and neural interfaces [5]. The provided approach, could be also used to infer information to enhance more specific regenerative models [6, 27, 29, 32, 33] accounting for the presence of regenerating axons or bundles [15]. Finally, the presented framework, exploiting a ”continuum mechanics approach”, may be coupled with enhanced researches [21, 23] aiming at combining in-vitro, in-vivo and in-human studies to investigate the ef-

fects of the surrounding environment (e.g., provided by artificial nerve-guides) on the nerve regeneration in peripheral nerve-gap lesions.

Figure Captions

Figure 1: Scheme of experimental set-up. a) Testing machine. b) Frontal and side view of the nerve specimen. c) Experimental data.

Figure 2: Behaviour of the reference cylindroid: a) Field of axial displacements. b) Field of axial stress. c) Comparison between the experimental and the in silico stress as a function of stretch ($R^2 \sim 0.9$). d) Percentage error between in silico and experimental data for axial stress. e) Comparison between in silico and theoretical transversal stretch. f) Difference between in silico and theoretical transversal stretch as a function of the axial stretch.

Figure 3: Approximation of the cylindrical model with a parallelepiped and a bi-dimensional model. a) Axial displacement of three-dimensional and bi-dimensional approximations. b) Stress fields of three-dimensional and bi-dimensional approximations.

Figure 4: Approximation of the reference cylindroid with a parallelepiped and with bi-dimensional plane models. a) Stress fields of three-dimensional and bi-dimensional approximations with respect to the reference cylindroid. b) Percentage errors among axial stresses in three-dimensional and bidimensional approximations with respect to the reference cylindroid. c) Comparison among of transversal stretches derived from different approximations: all lines are superimposed to the theoretical one d) Difference among three-dimensional and bi-dimensional approximations with respect to the theoretical transversal stretch.

Figure 5: a) Percentage decrease of computational time with the variation of material compressibility. The decrease is normalized with respect to the time needed to solve the fully incompressible reference cylindroid. b) Percentage decrease of computational time with the variation of the material compressibility. The decrease is normalized with respect to the time needed to solve the fully incompressible parallelepiped. c) Percentage decrease of computational time with the variation of the material compressibility for plane stress with thickness. The decrease is normalized with respect to the time needed to solve the respective fully incompressible bi-dimensional plane model. d) Percentage decrease of computational

time with the variation of the compressibility parameter for plane stress without thickness. The decrease is normalized with respect to the time needed to solve the respective fully incompressible plane model. e) Global percentage of time decrease for all approximation with respect to the fully incompressible reference cylindroid as a function of the compressibility of the material.

Figure 6: Effects of small width changes of a bi-dimensional model: a) The number of nodes and elements as a function of width. b) Variation of the time (normalized with respect to the reference width = 9.05 mm) with the changes of width for a fully incompressible material. b) Variation of the time (normalized with respect to the reference width = 9.05 mm) with the changes of width for a near incompressible material ($d = 1E-007$).

References

1. Alexander, M.J., Barkmeier-Kraemer, J.M., Vande Geest, J.P.: Biomechanical properties of recurrent laryngeal nerve in the piglet. Ann Biomed Eng **38**(8), 2553–2562 (2010). DOI 10.1007/s10439-010-0013-7. URL http://dx.doi.org/10.1007/s10439-010-0013-7
2. Anderson, A.E., Peters, C.L., Tuttle, B.D., Weiss, J.A.: Subject-specific finite element model of the pelvis: Development, validation and sensitivity studies. Journal of Biomechanical Engineering **127**(3), 364–373 (2005). DOI 10.1115/1.1894148. URL http://dx.doi.org/10.1115/1.1894148
3. Bell, M.A., Weddell, A.G.: A descriptive study of the blood vessels of the sciatic nerve in the rat, man and other mammals. Brain **107 (Pt 3)**, 871–898 (1984)
4. Caouette, C., Ikin, N., Villemure, I., Arnoux, P.J., Rauch, F., Aubin, C.É.: Geometry reconstruction method for patient-specific finite element models for the assessment of tibia fracture risk in osteogenesis imperfecta. Medical & Biological Engineering & Computing **55**(4), 549–560 (2017). DOI 10.1007/s11517-016-1526-5. URL https://doi.org/10.1007/s11517-016-1526-5
5. Carpaneto, J., Cutrone, A., Bossi, S., Sergi, P.N., Citi, L., Rigosa, J., Rossini, P., Micera, S.: Activities on pns neural interfaces for the control of hand prostheses. In: Engineering

in Medicine and Biology Society, EMBC, 2011 Annual International Conference of the IEEE, pp. 4637–4640 (2011). DOI 10.1109/IEMBS.2011.6091148

6. Ciofani, G., Sergi, P.N., Carpaneto, J., Micera, S.: A hybrid approach for the control of axonal outgrowth: preliminary simulation results. Med Biol Eng Comput **49**(2), 163–170 (2011). DOI 10.1007/s11517-010-0687-x. URL http://dx.doi.org/10.1007/s11517-010-0687-x
7. Clarke, E., Bearn, J.G.: The spiral nerve bands of fontana. Brain **95**(1), 1–20 (1972). DOI 10.1093/brain/95.1.1. URL + http://dx.doi.org/10.1093/brain/95.1.1
8. Cutrone, A., Sergi, P.N., Bossi, S., Micera, S.: Modelization of a self-opening peripheral neural interface: a feasibility study. Med Eng Phys **33**(10), 1254–1261 (2011). DOI 10.1016/j.medengphy.2011.06.001. URL http://dx.doi.org/10.1016/j.medengphy.2011.06.001
9. Dilley, A., Lynn, B., Greening, J., DeLeon, N.: Quantitative in vivo studies of median nerve sliding in response to wrist, elbow, shoulder and neck movements. Clinical Biomechanics **18**(10), 899 – 907 (2003). DOI http://dx.doi.org/10.1016/S0268-0033(03)00176-1. URL http://www.sciencedirect.com/science/article/pii/S0268003303001761
10. Dilley, A., Summerhayes, C., Lynn, B.: An in vivo investigation of ulnar nerve sliding during upper limb movements. Clinical Biomechanics **22**(7), 774 – 779 (2007). DOI http://dx.doi.org/10.1016/j.clinbiomech.2007.04.004. URL http://www.sciencedirect.com/science/article/pii/S0268003307000691
11. Duchemin, L., Mitton, D., Jolivet, E., , Bousson, V., , Laredo, J.D., , Skalli, W.: An anatomical subject-specific fe-model for hip fracture load prediction. Computer Methods in Biomechanics and Biomedical Engineering **11**(2), 105–111 (2008). DOI 10.1080/10255840701535965. URL http://dx.doi.org/10.1080/10255840701535965. PMID: 17891675
12. Fung, Y.C.: Biomechanics, Mechanical Properties of Living Tissues (1993)
13. Galardi, G., Comi, G., Lozza, L., Marchettini, P., Novarina, M., Facchini, R., Paronzini, A.: Peripheral nerve damage during limb lengthening. neurophysiology in five cases

of bilateral tibial lengthening. Bone & Joint Journal **72-B**(1), 121–124 (1990). URL http://bjj.boneandjoint.org.uk/content/72-B/1/121

14. Gardiner, J.C., Weiss, J.A.: Subject-specific finite element analysis of the human medial collateral ligament during valgus knee loading. Journal of Orthopaedic Research **21**(6), 1098–1106 (2003). DOI 10.1016/S0736-0266(03)00113-X. URL http://dx.doi.org/10.1016/S0736-0266(03)00113-X
15. Giannessi, E., Stornelli, M.R., Sergi, P.N.: A unified approach to model peripheral nerves across different animal species. PeerJ **5**, e4005 (2017). DOI 10.7717/peerj.4005. URL https://doi.org/10.7717/peerj.4005
16. Gubin, A.V., Borzunov, D.Y., Malkova, T.A.: The ilizarov paradigm: thirty years with the ilizarov method, current concerns and future research. International Orthopaedics **37**(8), 1533–1539 (2013). DOI 10.1007/s00264-013-1935-0. URL https://doi.org/10.1007/s00264-013-1935-0
17. Haninec, P.: Undulating course of nerve fibres and bands of fontana in peripheral nerves of the rat. Anatomy and Embryology **174**(3), 407–411 (1986). DOI 10.1007/BF00698791. URL https://doi.org/10.1007/BF00698791
18. Ma, Z., Hu, S., Tan, J.S., Myer, C., Njus, N.M., Xia, Z.: In vitro and in vivo mechanical properties of human ulnar and median nerves. J Biomed Mater Res A **101**(9), 2718–2725 (2013). DOI 10.1002/jbm.a.34573. URL http://dx.doi.org/10.1002/jbm.a.34573
19. Main, E.K., Goetz, J.E., Rudert, M.J., Goreham-Voss, C.M., Brown, T.D.: Apparent transverse compressive material properties of the digital flexor tendons and the median nerve in the carpal tunnel. J Biomech **44**(5), 863–868 (2011). DOI 10.1016/j.jbiomech.2010.12.005. URL http://dx.doi.org/10.1016/j.jbiomech.2010.12.005
20. Marchelli, G.L.S., Ledoux, W.R., Isvilanonda, V., Ganter, M.A., Storti, D.W.: Joint-specific distance thresholds for patient-specific approximations of articular cartilage modeling in the first ray of the foot. Medical & Biological Engineering & Computing **52**(9), 773–779 (2014). DOI 10.1007/s11517-014-1179-1. URL https://doi.org/10.1007/s11517-014-1179-1

21. Merolli, A.: Modelling peripheral nerve from studies on ”the bands of fontana” and on ”artificial nerve-guides” suggests a new recovery mechanism which can concur with brain plasticity. American Journal of Neuroprotection and Neuroregeneration **8**(1), 45–53 (2016). DOI doi:10.1166/ajnn.2016.1123
22. Merolli, A., Mingarelli, L., Rocchi, L.: A more detailed mechanism to explain the bands of fontana in peripheral nerves. Muscle and Nerve **46**(4), 540–547 (2012). DOI 10.1002/mus.23422. URL http://dx.doi.org/10.1002/mus.23422
23. Merolli, A., Rocchi, L., Wang, X.M., Cui, F.Z.: Peripheral nerve regeneration inside collagen-based artificial nerve guides in humans. Journal of Applied Biomaterials & Functional Materials **13**(1), 0–0 (2015). URL http://www.jabfm.com/article/peripheral-nerve-regeneration-inside-collagen-based-artificial-nerve-guides-in-humans
24. Millesi, H., Zoch, G., Reihsner, R.: Mechanical properties of peripheral nerves. Clin Orthop Relat Res (314), 76–83 (1995)
25. Mueller, M.J., Maluf, K.S.: Tissue adaptation to physical stress: A proposed physical stress theory to guide physical therapist practice, education, and research. Physical Therapy **82**(4), 383–403 (2002). URL http://ptjournal.apta.org/content/82/4/383.abstract
26. Pomwenger, W., Entacher, K., Resch, H., Schuller-Götzburg, P.: Multi-patient finite element simulation of keeled versus pegged glenoid implant designs in shoulder arthroplasty. Medical & Biological Engineering & Computing **53**(9), 781–790 (2015). DOI 10.1007/s11517-015-1286-7. URL https://doi.org/10.1007/s11517-015-1286-7
27. Roccasalvo, I.M., Micera, S., Sergi, P.N.: A hybrid computational model to predict chemotactic guidance of growth cones. Scientific Reports **5**, 11,340– (2015). URL http://dx.doi.org/10.1038/srep11340
28. Sergi, P.N., Carrozza, M.C., Dario, P., Micera, S.: Biomechanical characterization of needle piercing into peripheral nervous tissue. IEEE Trans Biomed Eng **53**(11), 2373–2386 (2006). DOI 10.1109/TBME.2006.879463. URL http://dx.doi.org/10.1109/TBME.2006.879463

29. Sergi, P.N., Cavalcanti-Adam, E.A.: Biomaterials and computation: a strategic alliance to investigate emergent responses of neural cells. Biomater. Sci. **5**, 648–657 (2017). DOI 10.1039/C6BM00871B. URL http://dx.doi.org/10.1039/C6BM00871B

30. Sergi, P.N., Jensen, W., Micera, S., Yoshida, K.: In vivo interactions between tungsten microneedles and peripheral nerves. Med Eng Phys **34**(6), 747–755 (2012). DOI 10.1016/j.medengphy.2011.09.019. URL http://dx.doi.org/10.1016/j.medengphy.2011.09.019

31. Sergi, P.N., Jensen, W., Yoshida, K.: Interactions among biotic and abiotic factors affect the reliability of tungsten microneedles puncturing in vitro and in vivo peripheral nerves: A hybrid computational approach. Materials Science and Engineering: C **59**, 1089 – 1099 (2016). DOI http://dx.doi.org/10.1016/j.msec.2015.11.022. URL http://www.sciencedirect.com/science/article/pii/S0928493115305531

32. Sergi, P.N., Marino, A., Ciofani, G.: Deterministic control of mean alignment and elongation of neuron-like cells by grating geometry: a computational approach. Integr. Biol. **7**, 1242–1252 (2015). DOI 10.1039/C5IB00045A. URL http://dx.doi.org/10.1039/C5IB00045A

33. Sergi, P.N., Morana Roccasalvo, I., Tonazzini, I., Cecchini, M., Micera, S.: Cell guidance on nanogratings: a computational model of the interplay between pc12 growth cones and nanostructures. PLoS One **8**(8), e70,304 (2013). DOI 10.1371/journal.pone.0070304. URL http://dx.doi.org/10.1371/journal.pone.0070304

34. Shim, V.B., Fernandez, J.W., Gamage, P.B., Regnery, C., Smith, D.W., Gardiner, B.S., Lloyd, D.G., Besier, T.F.: Subject-specific finite element analysis to characterize the influence of geometry and material properties in achilles tendon rupture. Journal of Biomechanics **47**(15), 3598 – 3604 (2014). DOI http://dx.doi.org/10.1016/j.jbiomech.2014.10.001. URL http://www.sciencedirect.com/science/article/pii/S002192901400520X

35. Smith, J.: Factors influencing nerve repair: I. blood supply of peripheral nerves. Archives of Surgery **93**(2), 335–341 (1966). DOI 10.1001/archsurg.1966.01330020127022. URL +

http://dx.doi.org/10.1001/archsurg.1966.01330020127022

36. Smith, J.: Factors influencing nerve repair: Ii. collateral circulation of peripheral nerves. Archives of Surgery **93**(3), 433–437 (1966). DOI 10.1001/archsurg.1966.01330030063014. URL + http://dx.doi.org/10.1001/archsurg.1966.01330030063014
37. Stanton-Hicks, M.: Chapter 29 - peripheral nerve stimulation for pain peripheral neuralgia and complex regional pain syndrome. In: E.S. Krames, P.H. Peckham, A.R. Rezai (eds.) Neuromodulation, pp. 397 – 407. Academic Press, San Diego (2009). DOI https://doi.org/10.1016/B978-0-12-374248-3.00030-6. URL https://www.sciencedirect.com/science/article/pii/B9780123742483000306
38. Sunderland, S.: The intraneural topography of the radial, median and ulnar nerves. Brain **68**, 243–299 (1945)
39. Sunderland, S.: The connective tissues of peripheral nerves. Brain **88**(4), 841–854 (1965)
40. Tarjuelo-Gutierrez, J., Rodriguez-Vila, B., Pierce, D.M., Fastl, T.E., Verbrugghe, P., Fourneau, I., Maleux, G., Herijgers, P., Holzapfel, G.A., Gomez, E.J.: High-quality conforming hexahedral meshes of patient-specific abdominal aortic aneurysms including their intraluminal thrombi. Medical & Biological Engineering & Computing **52**(2), 159–168 (2014). DOI 10.1007/s11517-013-1127-5. URL https://doi.org/10.1007/s11517-013-1127-5
41. Topp, K.S., Boyd, B.S.: Structure and biomechanics of peripheral nerves: nerve responses to physical stresses and implications for physical therapist practice. Phys Ther **86**(1), 92–109 (2006)
42. Williams, M.J., Utzinger, U., Barkmeier-Kraemer, J.M., Vande Geest, J.P.: Differences in the microstructure and biomechanical properties of the recurrent laryngeal nerve as a function of age and location. Journal of Biomechanical Engineering **136**(8), 0810,081–0810,089 (2014). URL http://www.ncbi.nlm.nih.gov/pmc/articles/PMC4056420/
43. Yoshida, K., Lewinsky, I., Nielsen, M., Hylleberg, M.: Implantation mechanics of tungsten microneedles into peripheral nerve trunks. Med Biol Eng Comput **45**(4), 413–420

(2007). DOI 10.1007/s11517-007-0175-0. URL http://dx.doi.org/10.1007/s11517-007-0175-0

44. Zachary, L.S., Dellon, E.S., Nicholas, E.M., Dellon, A.L.: The structural basis of felice fontana's spiral bands and their relationship to nerve injury. J reconstr Microsurg **9**(02), 131–138– (1993)
45. Zochodne, D.W., Low, P.A.: Adrenergic control of nerve blood flow. Exp Neurol **109**(3), 300–307 (1990)

Acknowledgements

The authors thank the company "Desideri Luciano s.r.l" for biological specimens and Dr. Cesare Temporin for his valuable technical assistance in handling and dissection of peripheral nerves.

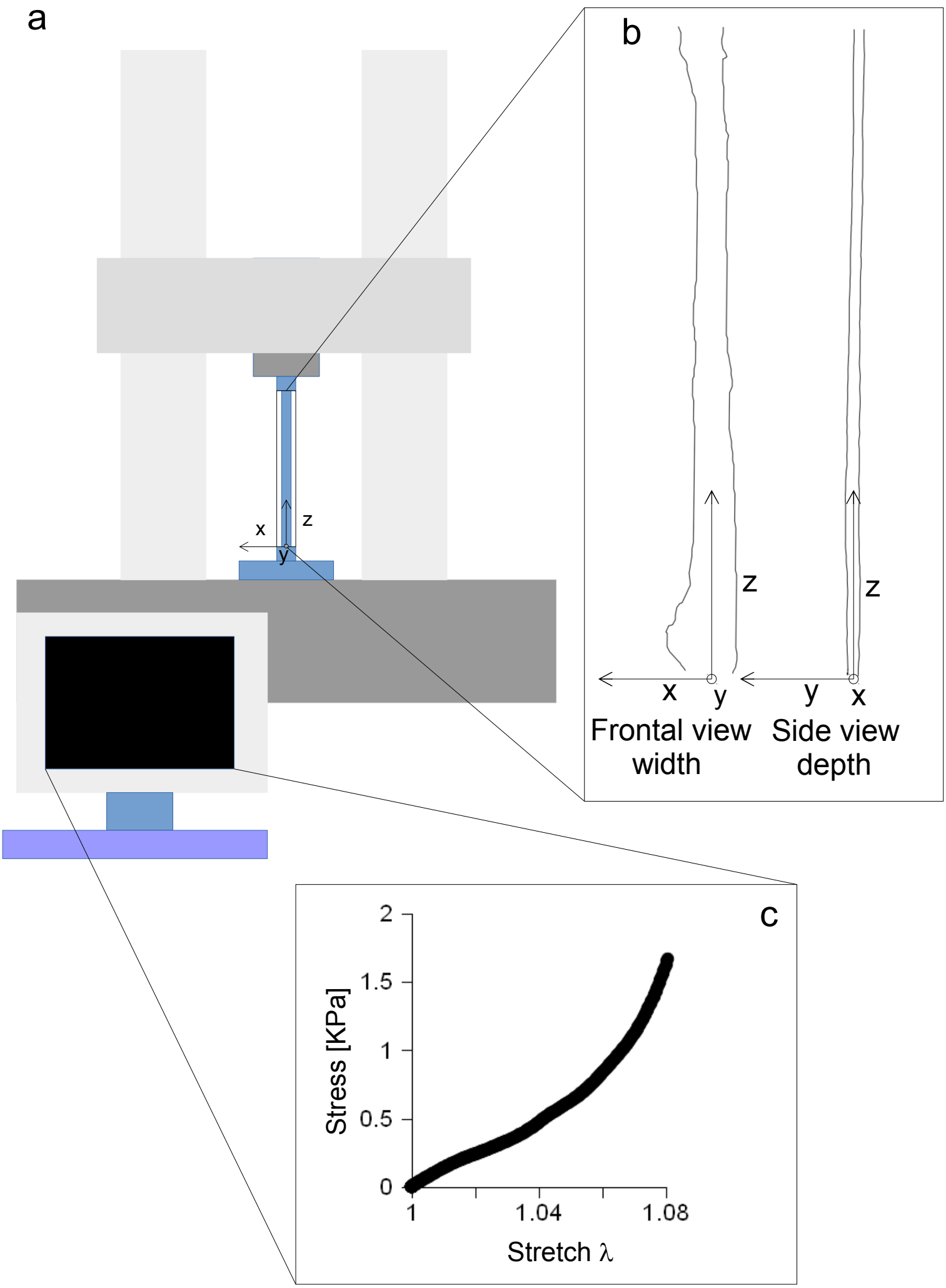
a
b
x
z
y
z
z
x
y
y
x
Frontal view
width
Side view
depth
c
2
1.5
1
0.5
0
Stress [KPa]
1
1.04
1.08
Stretch λ

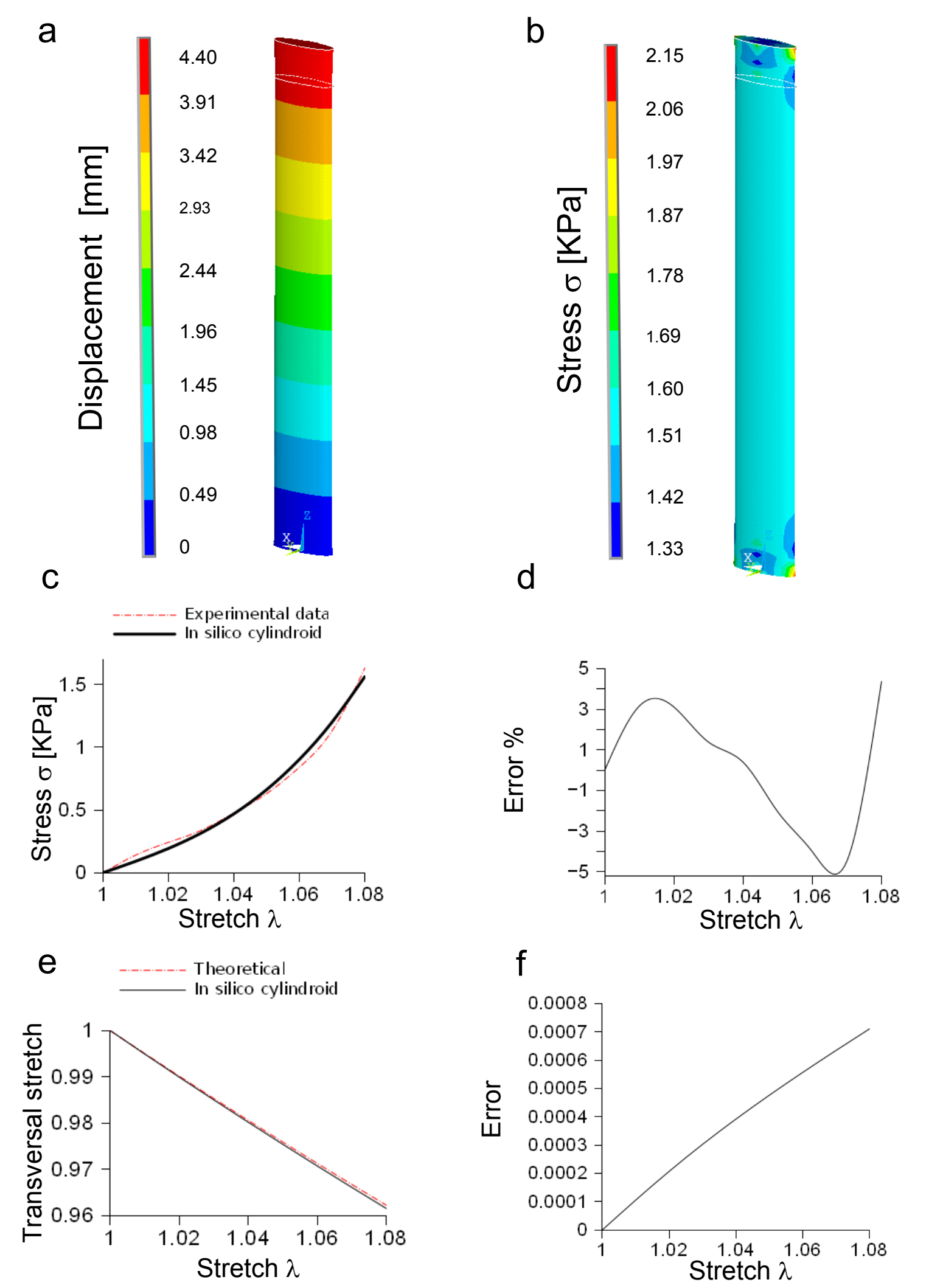
a
Displacement [mm]
4.40
3.91
3.42
2.93
2.44
1.96
1.45
0.98
0.49
0
b
Stress σ [KPa]
2.15
2.06
1.97
1.87
1.78
1.69
1.60
1.51
1.42
1.33
c
Experimental data
In silico cylindroid
Stress σ [KPa]
Stretch λ
d
Error %
Stretch λ
e
Theoretical
In silico cylindroid
Transversal stretch
Stretch λ
f
Error
Stretch λ

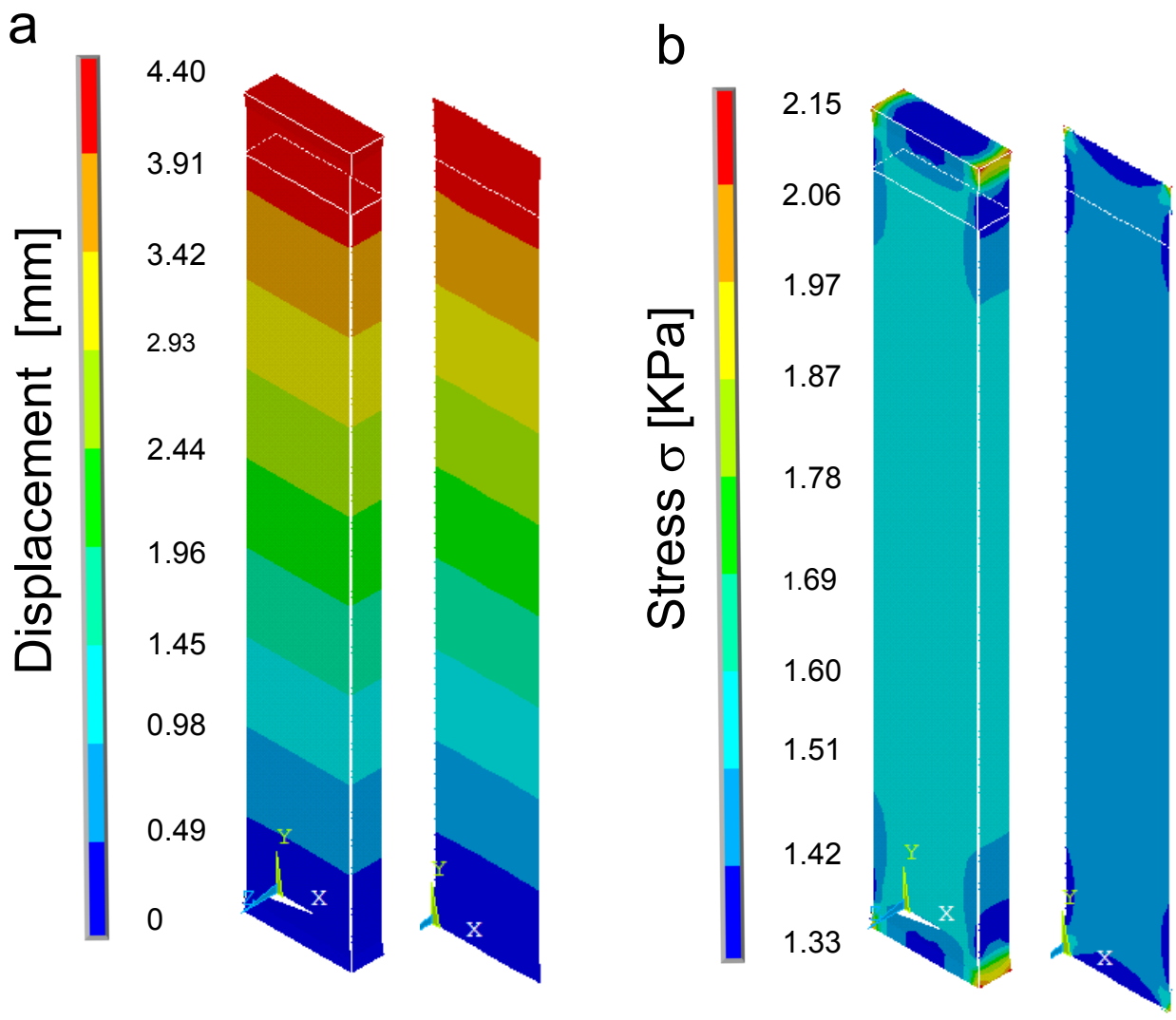
a
Displacement [mm]
4.40
3.91
3.42
2.93
2.44
1.96
1.45
0.98
0.49
0
b
Stress σ [KPa]
2.15
2.06
1.97
1.87
1.78
1.69
1.60
1.51
1.42
1.33

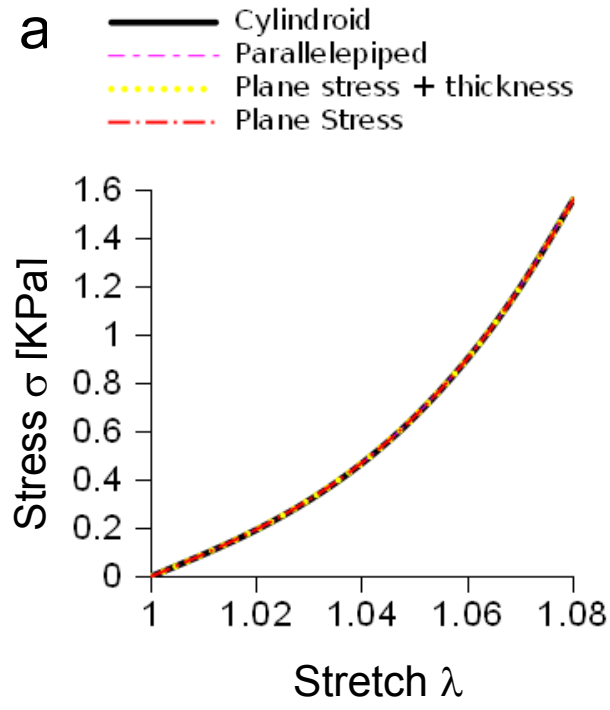
a
Cylindroid
Parallelepiped
Plane stress + thickness
Plane Stress
Stress σ [KPa]
1.6
1.4
1.2
1
0.8
0.6
0.4
0.2
0
1
1.02
1.04
1.06
1.08
Stretch λ

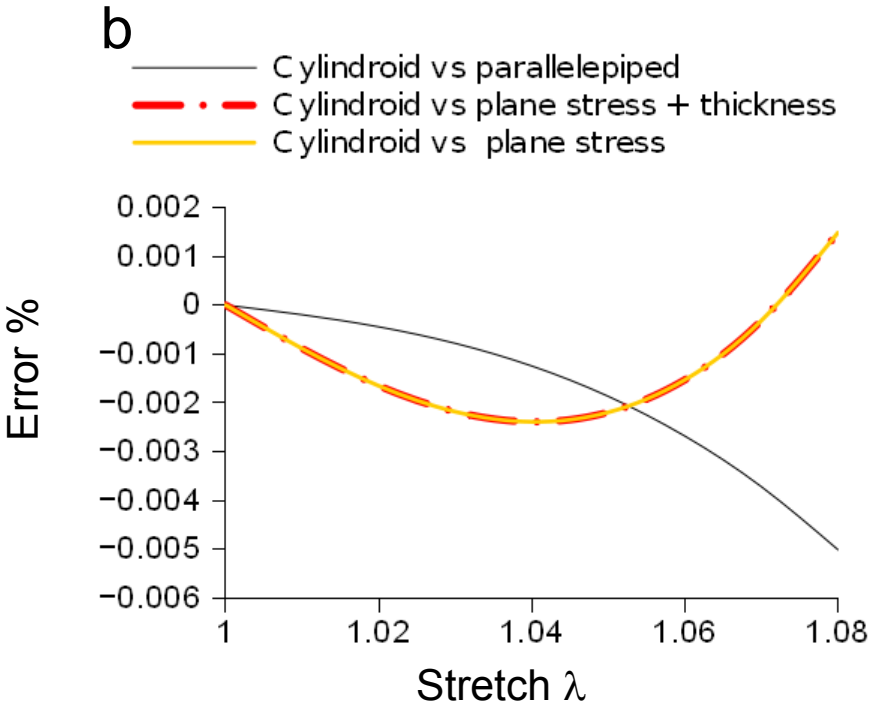
b
Cylindroid vs parallelepiped
Cylindroid vs plane stress + thickness
Cylindroid vs plane stress
Error %
0.002
0.001
0
−0.001
−0.002
−0.003
−0.004
−0.005
−0.006
1
1.02
1.04
1.06
1.08
Stretch λ

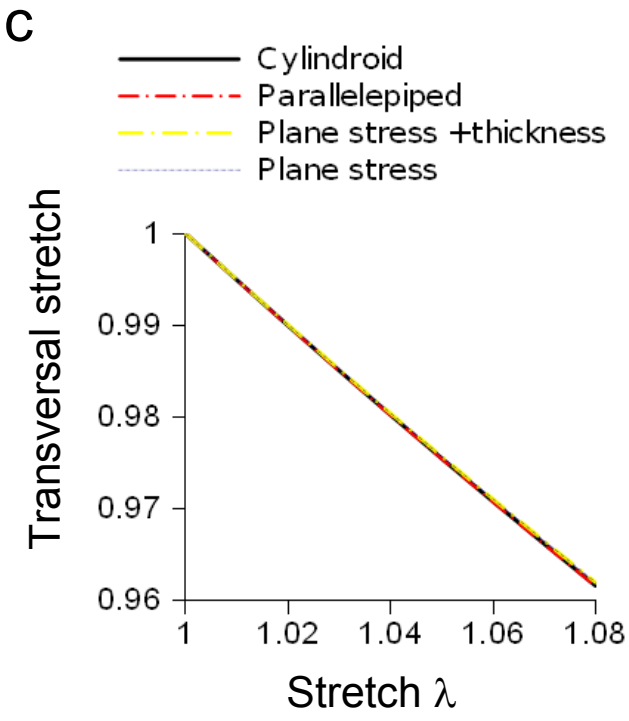
c
Cylindroid
Parallelepiped
Plane stress +thickness
Plane stress
Transversal stretch
1
0.99
0.98
0.97
0.96
1
1.02
1.04
1.06
1.08
Stretch λ

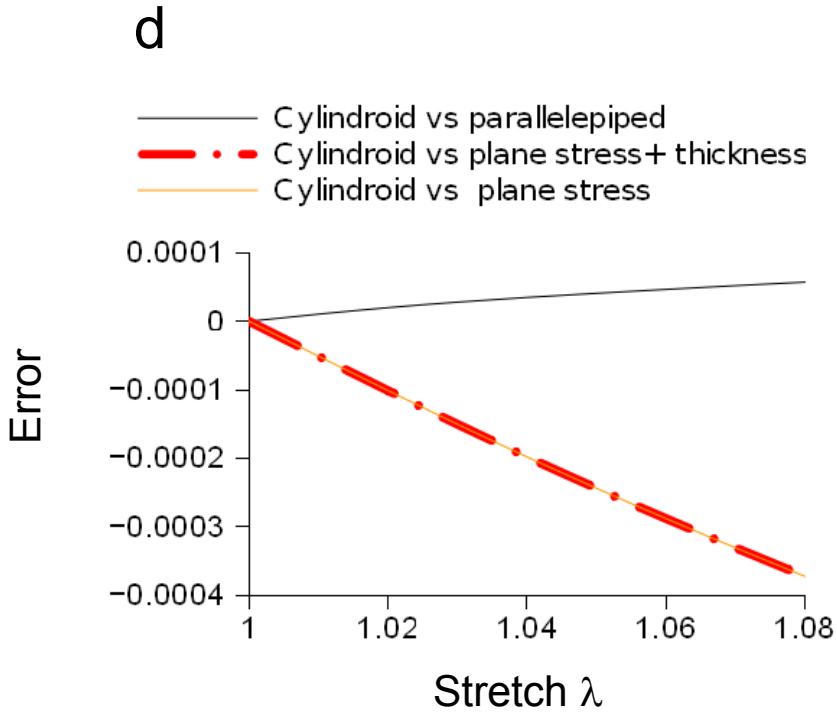
d
Cylindroid vs parallelepiped
Cylindroid vs plane stress+ thickness
Cylindroid vs plane stress
Error
0.0001
0
−0.0001
−0.0002
−0.0003
−0.0004
1
1.02
1.04
1.06
1.08
Stretch λ

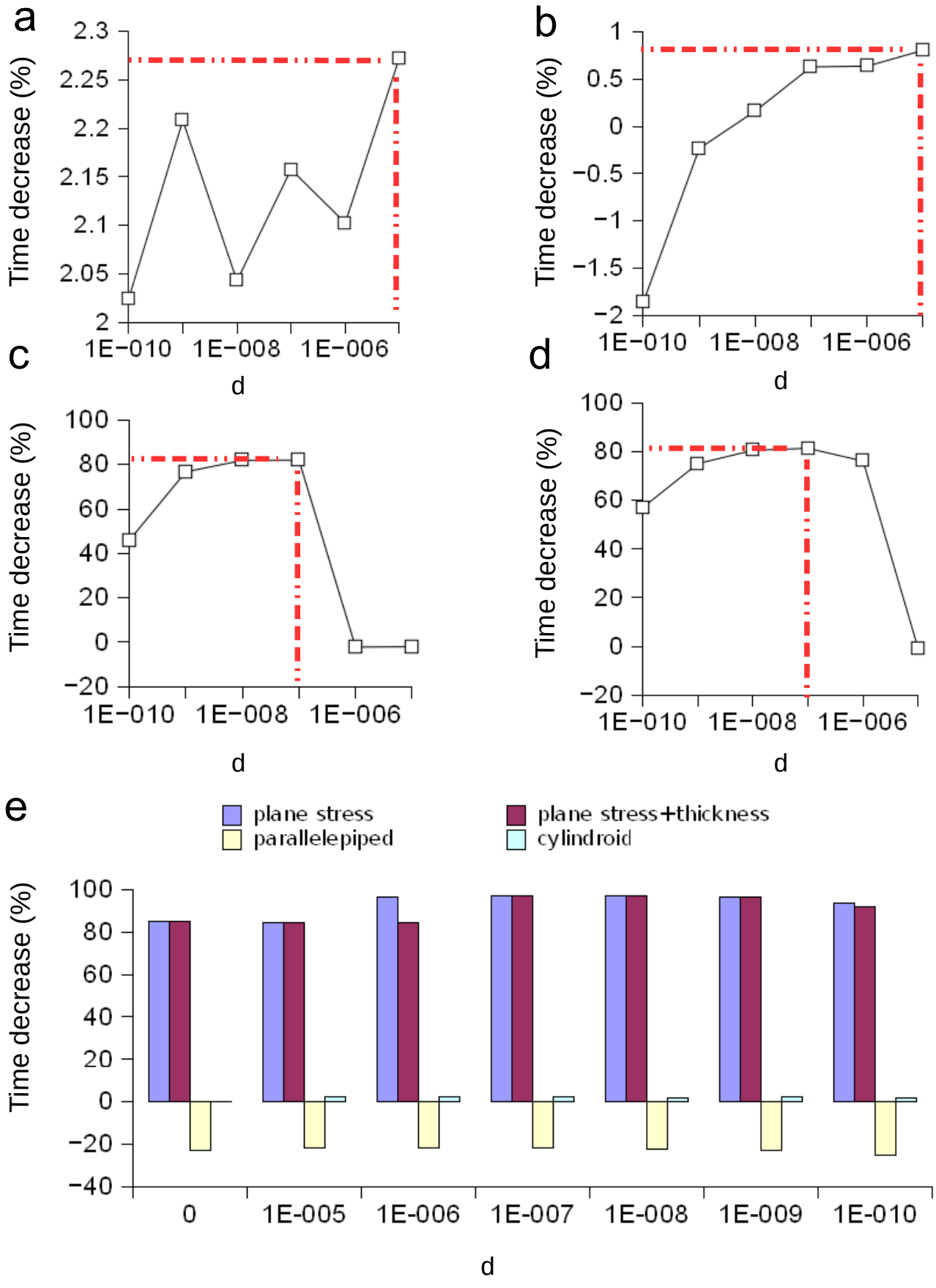
a
Time decrease (%)
2.3
2.25
2.2
2.15
2.1
2.05
2
1E−010
1E−008
1E−006
d
b
Time decrease (%)
1
0.5
0
−0.5
−1
−1.5
−2
1E−010
1E−008
1E−006
d
c
Time decrease (%)
100
80
60
40
20
0
−20
1E−010
1E−008
1E−006
d
d
Time decrease (%)
100
80
60
40
20
0
−20
1E−010
1E−008
1E−006
d
e
plane stress
parallelepiped
plane stress+thickness
cylindroid
Time decrease (%)
100
80
60
40
20
0
−20
−40
0
1E-005
1E-006
1E-007
1E-008
1E-009
1E-010
d

a

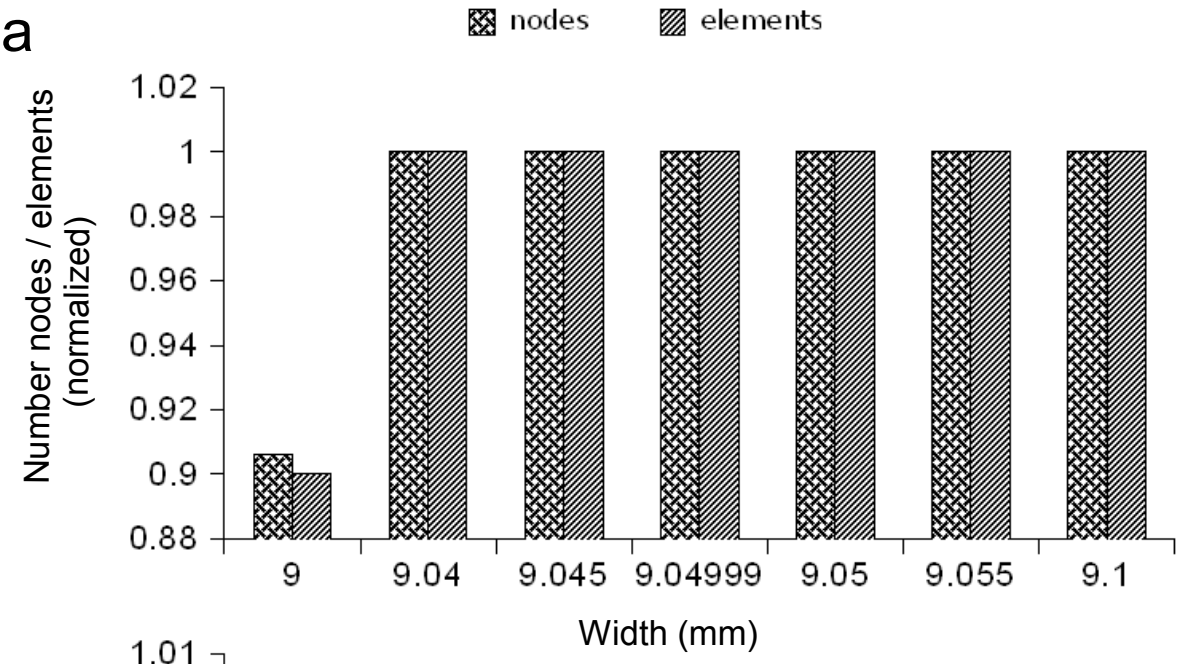
nodes
elements
Number nodes / elements (normalized)
1.02
1
0.98
0.96
0.94
0.92
0.9
0.88
9
9.04
9.045
9.04999
9.05
9.055
9.1
Width (mm)

b

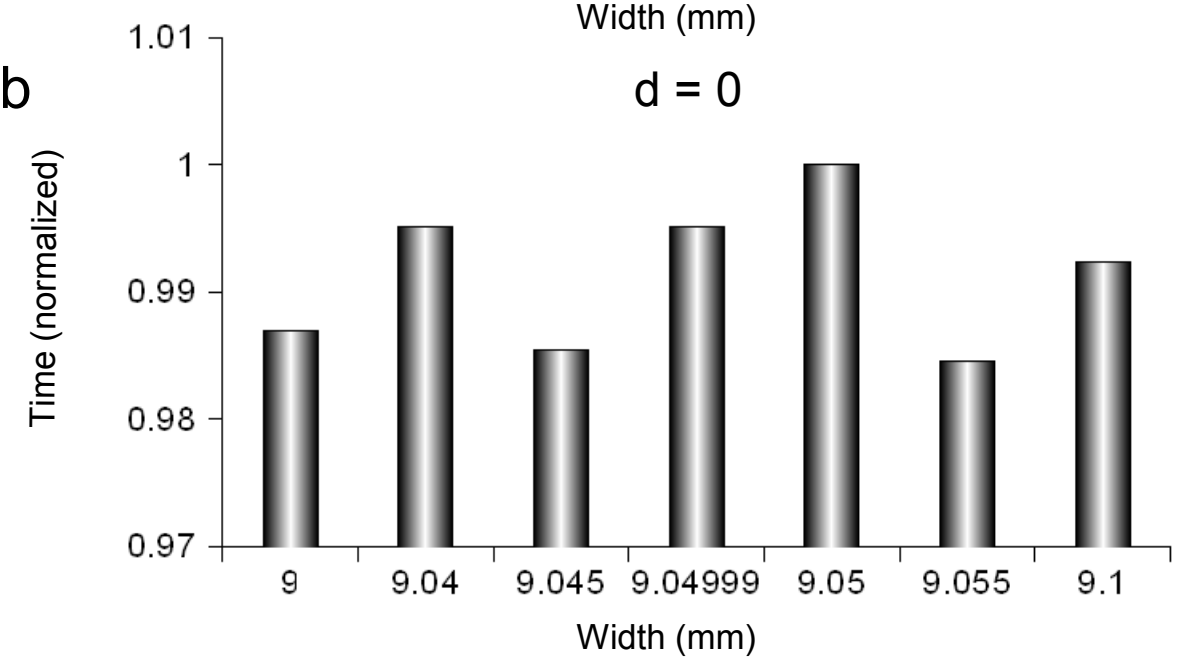
d = 0
Time (normalized)
1.01
1
0.99
0.98
0.97
9
9.04
9.045
9.04999
9.05
9.055
9.1
Width (mm)

c

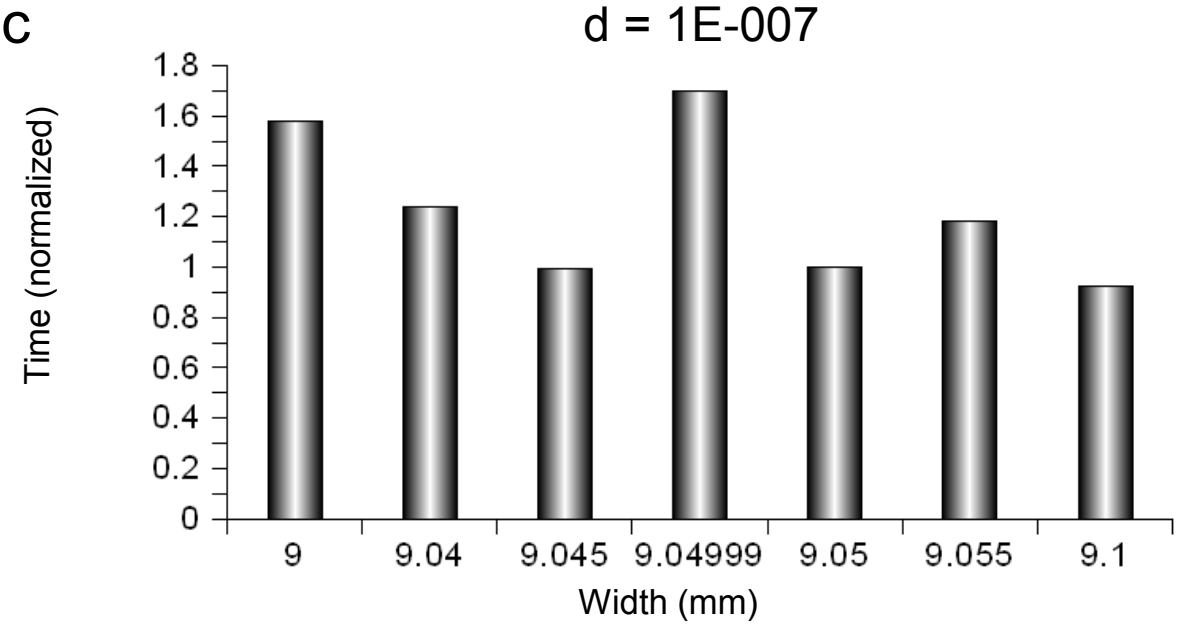
d = 1E-007
Time (normalized)
1.8
1.6
1.4
1.2
1
0.8
0.6
0.4
0.2
0
9
9.04
9.045
9.04999
9.05
9.055
9.1
Width (mm)